A MULTIWIRE VETO DETECTOR FOR THE HALL A

THIRD ARM AT THE

THOMAS JEFFERSON NATIONAL ACCELERATOR FACILITY

by

JESSE BERNARD HINES

(Under the Direction of F. Todd Baker and Uwe Happek)

ABSTRACT

Presented is the design, construction, testing and analysis of a multiwire veto chamber constructed for use in a third arm at the Thomas Jefferson National Accelerator Facility. The purpose of the veto chamber was to detect charged particles that are difficult to differentiate from photons in the calorimeter. Charged particles deposit energy in the chamber along their path thereby ionizing the chamber gas. The ions drift towards the cathode and the electrons, in turn, are amplified in the region close to the wires. The current pulse is detected and recorded electronically. Photons are not easily detected by the chamber due to their low probability of interaction with the chamber gas. I present an analysis of actual experimental data obtained that demonstrates that the wire chamber efficiency of detecting charged particles was better than 96% and that the chamber was effective in providing calibration data for the segmented lead glass calorimeter.

INDEX WORDS: nuclear physics, CEBAF, TJNAF, MWPC, wire chamber, particle detector, real compton scattering

A MULTIWIRE VETO DETECTOR FOR THE HALL A THIRD ARM AT THE THOMAS JEFFERSON NATIONAL ACCELERATOR FACILITY

by

JESSE BERNARD HINES

B.S. Physics, State University of West Georgia, 1996

A Thesis Submitted to the Graduate Faculty of The University of Georgia in Partial Fulfillment of the Requirements for the Degree

MASTER OF SCIENCE

ATHENS, GEORGIA

2004

© 2004

Jesse Bernard Hines

All Rights Reserved

A MULTIWIRE VETO DETECTOR FOR THE HALL A THIRD ARM AT THE THOMAS JEFFERSON NATIONAL ACCELERATOR FACILITY

by

JESSE BERNARD HINES

Major Professors: F. Todd Baker
Uwe Happek

Committee: F. Todd Baker
Uwe Happek
Steven Lewis

Electronic Version Approved:

Maureen Grasso
Dean of the Graduate School
The University of Georgia
August 2004

TABLE OF CONTENTS

CHAPTER 1

INTRODUCTION

The goal of this project was to design a veto detector for use in the real Compton scattering experiment at Jefferson Lab. The accelerator at Jefferson Labs provides an electron beam source operating at up to 12 GeV. There already exists in Hall A two high resolution spectrometers that are equipped to measure the scattering angle and momentum of scattered protons and electrons. The real Compton scattering experiment required the construction of a third arm to measure the scattering angle and momentum of a scattered photon.

Electrons and photons are difficult to distinguish in the calorimeter. The veto detectors are designed to detect the passage of an electron in order discriminate between the two.

The experimental setup for the third arm consisted of four detectors in addition to the segmented calorimeter. The purpose of the other four detectors were to act as veto detectors for charged particles. The detectors in order from closest to the target to the calorimeter are: the gas cherenkov, segmented lead glass veto, scintillator paddle and the wire chamber.

My goal was to design a wire chamber that would detect efficiently charged particles and also provide a calibration source for the calorimeter.

CHAPTER 2

THEORY

Particle Interactions With Matter

Charged particles and photons interact with matter differently. Photons are destroyed by their first interaction resulting in an electromagnetic shower in contrast to the passage of charged particles that interact with and ionize the chamber gas along their path. We desire that the shower occur in the calorimeter so that it is completely contained. The 5.9 KeV photons emitted by an 55Fe source each produce on average 227 electron ion pairs as a single cluster [6]. Charged particles ionize the gas along their path resulting in electron-ion pairs along their track. This ionization is not uniform along the path but instead is in clusters. Regardless of the interaction, the detection of particles and photons requires the detection of the ionization of the gas.

It is possible to estimate the number of electrons in all of the clusters along an ionization track due to the passage of minimum ionizing particles such as beta rays from a 90Sr source. A minimum ionizing particle passing through the gas interacts randomly with the gas molecules a few electrons from each collision. These electrons are referred to as primary electrons and themselves generally have enough kinetic energy to ionize nearby gas molecules. The ion itself can interact with other gas components to produce additional ions also. The electrons and ions formed from the primary collision thus result in a cluster which contains on average approximately 20 electrons.

Multiplication Factor (Gas Gain)

To detect the passage of particles it is necessary to separate the electrons and ions. The method employed is to apply a large potential difference between the cathode and the wires. This field separates the electron-ion pairs by causing the ions to drift towards the cathode and the electrons to the wires. In the region close to the wires the field is large enough that the electrons can gain enough energy between collisions to produce additional electron-ion pairs by ionizing the chamber gas. The electrons that are produced by ionizing the gas are themselves accelerated ionizing additional gas molecules. The result is an avalanche of electrons arriving at the sense wires. Typical avalanches produce 10^4 to 10^7 electrons from a single electron.

The magnitude of this avalanche is referred to as the gain or multiplication factor of the chamber. The gain is dependent upon the shape and strength of the electric field between the anode wires and cathode. The majority of the gain occurs within a region of just a few wire diameters of the wire itself.

The number of electrons produced in the avalanche is calculated by integrating the first Townsend coefficient for the particular gas used in the chamber [9].

(2.1) $$\frac{N}{N_0} = \exp\left[\int_{r_a}^{r_{\min}} \alpha(r)dr\right]$$

Here r_a is the wire radius and r_{min} is the radius at which the electric field is large enough such that the kinetic energy of the electrons between collisions is greater than the energy required to ionize the gas. This equation does not take into account the reduction of the field due large numbers of electrons being accelerated towards the wire simultaneously.

The first prototype was constructed using components of a chamber designed by Howard Fenker. The chamber was originally designed for detecting individual beam particle trajectories for research at Fermilab [8]. The components removed from storage at the Stanford Linear Accelerator (SLAC) and assembled at UGA. The design consists of stacked planes of alternating high voltage and ground planes.

Table 2.1 Fenker chamber properties

Operating voltage	2700V (2850V)
Wire diameter	10μm
Wire spacing	1mm
Wire/cathode spacing	3mm
Active area	128mm x 128mm

Unfortunately the components had previously seen extensive use in the beam lines at SLAC and therefore proved to be unreliable. Wire breakage due to breakdown of the chamber was the most serious problem.

This chamber still proved itself useful in that it demonstrated that a multi-wire proportional chamber (MWPC) could survive in the open environment in Hall A. The chamber had 10 micron wires and 1 mm resolution. The active area was a 128 mm X 128 mm. This was not well-suited for the Compton scattering experiments since the active area of the chamber only covered a small fraction of the calorimeter. The 1 mm resolution of the wire chamber was unnecessary as the maximum resolution which has been obtained with the calorimeter is about 4 mm.

Repair techniques

The first prototype afforded us many opportunities to develop repair techniques that can be used on other chambers. Repairs to the chamber usually are the result of a broken wire/wires due to electrostatic discharge. The broken wire invariably ends up in contact with one of the cathodes resulting in a short circuit. It was found that we could determine which plane had a broken wire by connecting high voltage to single planes to test for this short circuit. In this way, we can plan which end of the chamber should be opened so that only half the chamber would need to be disassembled.

Since the wires are held in place by epoxy, it is necessary to cut away the epoxy holding the broken wire in place. This is usually done very carefully using a razor blade. Once the wire has been removed in the area in which the new wire is to be installed should be scraped smooth in order for the new wire to lie flat on the board.

It is important that the new wire be positioned very accurately. Sauli [4 p.55-56] has noted that in a chamber with 2 mm wire spacing and 20 micron wires that only a 0.1 mm displacement within the plane of the wires can result in more than a 10% change in the gas gain for that wire. A single wire with increased gain will limit the operating voltage of the chamber and could therefore limit the efficiency since efficiency is a function of the operating voltage.

We developed a novel approach to accurately align the replacement wires. The wire plane assembly is placed on overhead projector and the image of the wires is focused on a screen. An alignment template is made using the neighboring wires and then placed in the area where the replacement wires are to be inserted. Using this technique, the 1mm spacing it is enlarged to 2 cm on the screen. It then becomes quite an easy task to position the new wires to better than 0.1 mm accuracy.

CHAPTER 3

NEW DESIGN

Goal

The first prototype had shown us that it was possible to operate a wire chamber unshielded in Hall A. The first prototype also proved its worth as a calibration instrument for the other detectors but a larger more robust design was needed.

The 10 micron wires of the first prototype were exceedingly difficult to work with. Therefore it was decided that the new chamber should used more common 20 micron wires and that the wire spacing could be increased to 2 mm. The wire chamber should also cover four times the area of the first prototype. With these requirements in mind, the new wire chamber was designed.

Predicting the Gain

The multiplication factor can be determined by integrating the first Townsend coefficient. The Townsend coefficient is calculated by Garfield, a monte-carlo simulation of electron drift in wire chambers. It calls Magboltz that generates a gas profile data file from the cluster size distribution provided by the user.

The cluster size distribution for a gas mixture can be calculated from the cluster size distributions of the individual components using the equation

(3.1) $$w_{12} = \frac{\pi_1}{\pi_1 + \pi_2} w_1(n) + \frac{\pi_2}{\pi_1 + \pi_2} w_2(n)$$

where π_1 and π_2 are the partial pressures of components 1 and 2, multiplied by their corresponding primary ionization cross sections [1]. Partial pressures can be found simply by multiplying the pressure p of the mixture by the fraction f of each constituent [2].

(3.2) $$\pi = f\ p$$

The cluster size distribution is then read into GARFIELD which calls MAGBOLTZ and generates a gas profile data file. The Townsend coefficient is calculated by Garfield and output in both table and interpolated format.

Garfield generates the Townsend coefficient as a function of the reduced field E/p. In order to integrate α then it is necessary to first multiply E/p by the pressure which in our case is 760 torr.

The electric field for this chamber can be derived [4] and is found to be

(3.3) $$E(x, y) = \frac{CV_0}{2\pi\varepsilon_0 s}\left(\frac{1 + \tan^2\left(\pi\frac{x}{s}\right)\tanh^2\left(\pi\frac{y}{s}\right)}{\tan^2\left(\pi\frac{x}{s}\right) + \tanh^2\left(\pi\frac{y}{s}\right)}\right)^{1/2}$$

Using equation 3.3 we can calculate the gain as a function of the field for various gas mixtures.

Practical Design

The goal in designing the chamber is to detect charged particles efficiently. This requires that any minimum ionizing particle should result in a current pulse that is within the dynamic range of the amplifier cards. Realizing this, a suitable range of the multiplication factor can be calculated immediately for the particular card to be used.

The next task is to determine, based on the required wire spacing, which gas mixture should be used and what the gap between the cathode and the wires should be. A rule of thumb for the cathode spacing is that should be three times the wire spacing. Gas selection depends upon the application. Using the programs Garfield and Magboltz one can determine the first Townsend coefficient that can then be integrated to determine the multiplication factor. This results in the first the constraint on the gas and also fixes the maximum operating voltage.

The field at the surface of the cathode increases linearly with the inverse of the cathode to wire spacing. It must be insured that the field at the surface of the cathode does not exceed a maximum value above which breakdown can be initiated at the cathode at the normal operating voltage of the chamber.

Operating Voltage

Operating voltages of 3000-5000 volts are typically necessary to get the desired amplification. The higher the voltage the larger the gain and the larger the signal received by the amplifiers.

There is a limit to the voltage that can be applied to a chamber. Too high a voltage can cause a continuous discharge when the field at the surface of the wire exceeds the ionization potential of the gas. The chamber can be damaged or destroyed by the discharge by melting the wires and the cathode.

Gas Selection

Two of the common gas mixtures currently in use in wire chambers are Ar-CH4 (argon-ethane) and Ar-CO2 (argon-carbon dioxide). Ar-CH4 is commonly believed to yield higher gas gain than Ar-CO2 but is extremely flammable. In fact, Ar-CH4 and Ar-CO2 both yield similar gains in the amplification region around the wire as will be discussed shortly. Ar-CH4 has also been shown to form carbon deposits on the wires, as a result of chamber discharges or when exposed to high particle rates, which degrade the performance of the chamber over time.

The selection of the gas composition depends primarily on the electric field in the active region of the chamber and the desired drift properties. It has been determined [5] that the properties of ethane and CO2 in the amplification region are similar. Therefore the selection of quencher can be made to select the desired drift time properties outside of the amplification region.

Drift time properties are important if one wishes to determine the track position more accurately than the wire spacing or to determine the angle of the track through the chamber. This requires the use of time to digital converters (TDC's) that add significant expense to the readout electronics. Since the basic resolution of 2mm is adequate the extra expense was not warranted for the real compton scattering experiment.

Construction

To balance the electrical forces that deform the cathode and the wires it is necessary to add additional cathodes and ground planes. Significant displacements of the wires or cathodes can cause large gain variations. Recall that the gas gain is a function of the field at the wire. Small displacements of the wires can have a large effect on the field.

The addition of a cathode plane on the opposite side of the wires balances the forces on the wires. The addition of two ground planes or windows balances the forces on the cathodes.

It is best to have all active elements experience symmetric electric forces to minimize deformation of geometry.

There is one more problem concerning forces in the chamber. All the wires are repelling each other and, if they are not stretched tight enough, will deflect out-of-plane changing the gain. The wires should be stretched with the greatest tension possible in order to minimize this effect. In practice, there is a maximum tension that the wires can withstand. Chambers are typically required to cover large areas resulting in the use of long wires. The maximum tension that can be placed on a tungsten wire is given in Table 3.2.

Table 3.2 Yield strength of tungsten wire for several common wire diameters.

Diameter (um)	Tmax (N)
5	0.04
10	0.16
20	0.65
30	1.45

Wire diameters commonly used are 10 to 30 microns. The longer the wire and the closer the wire spacing the easier it will be to deflect out-of-plane. Sauli [4] has derived an equation for the critical stability length

$$L_c = \frac{s}{CV_0}\sqrt{4\pi\varepsilon_0 T_{\max}} \tag{3.4}$$

where the capacitance per unit length is given by

(3.5)
$$C = \frac{2\pi\varepsilon_0}{\left(\frac{\pi l}{s}\right) - \ln\left(\frac{2\pi a}{s}\right)}$$

Here s is the wire spacing, C is the capacitance per unit length, V is the voltage and T is the tension on the wire. Calculations of these various parameters are given in Table 3.2

Table 3.2 Field strength at the surface of the wire and the critical stability length for several chamber parameters.

Wire plane Thickness	Spacer Thickness	Wire Radius m	Wire Spacing m	Yield Strength N	Cathode Spacing m	Capacitance pF/m	Voltage V	Charge C/m	E at wire V/m	E at wire KV/cm	Critical Stability Length m
0.1250	0.1880	1.00E-05	2.00E-03	0.65	7.9502E-03	3.487E-12	3000	1.046E-08	1.881E+07	188	1.626
0.1250	0.1250	1.00E-05	2.00E-03	0.65	6.3500E-03	4.139E-12	3000	1.2417E-08	2.233E+07	223	1.369
0.0930	0.1250	1.00E-05	2.00E-03	0.65	5.5370E-03	4.574E-12	4000	1.8295E-08	3.290E+07	329	0.929
0.0930	0.0930	1.00E-05	2.00E-03	0.65	4.7244E-03	5.110E-12	4000	2.0441E-08	3.676E+07	368	0.832
0.0625	0.0625	5.00E-06	1.00E-03	0.17	3.1750E-03	4.139E-12	2700	1.118E-08	4.019E+07	402	0.389

At the wire.....

80-20 Townsend/p 1/cmTorr	Raether Condition ? =20	99-1 Townsend/p 1/cmTorr	Raether Condition ? =20
5.2615	1.0523	5.5321	1.1064
6.3677	1.2735	6.6293	1.3259
9.6900	1.9380	9.9251	1.9850
10.9030	2.1806	11.1284	2.2257
11.9823	1.1982	12.1991	1.2199

Wire chamber analysis.xls

Circuit board layout

The circuit boards were designed using AutoCAD. AutoCAD has the precision layout capability to design all the chamber planes and "stack" the chamber on the computer to verify correct alignment of all the components prior to actual assembly.

Once the design of the planes were completed the images of the circuit traces had to be converted to precision transparencies in order for the circuit boards to be produced. Each plane was printed as positives at twice actual size on a large format HP inkjet printer. The circuit board manufacturer in Atlanta then photographed these images and reduced them by 50 percent to produce the negatives required for the photoresist process. Printing at double size then reducing by 50 percent insured that the individual pixels in the printout would not be visible on the completed boards. This is important because the high voltages used in the wire chamber can easily jump from trace to trace if there are any sharp edges.

The circuit board material of the first prototype was G-10. This material was removed from common use due to its flammable nature [7]. The more modern FR-4 material was designed to overcome the flammability of G-10.

CHAPTER 4

INTERFACING WITH THE EXPERIMENT

Lead Glass Signals

Signals from the PMT's attached to the lead glass blocks are fed into ADC's and simultaneously to the trigger logic. The signals to the ADC's are delayed to allow for propagation delays in the trigger logic.

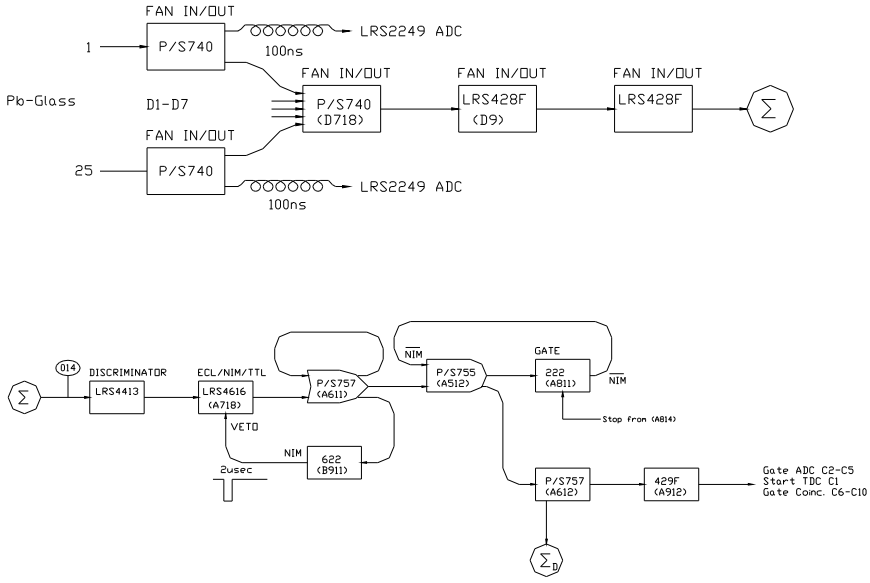

Figure 4.1 Calorimeter lead glass schematic. Shown are the delayed inputs to the ADC's and the trigger logic.

The trigger logic consists of a signal made up of a sum of all the signals from the photomultiplier tubes (PMT's). This sum is fed into a discriminator that outputs a trigger signal if the input exceeds a threshold value. This trigger signal is sent to analog to digital converters (ADC's) and the time to digital converters (TDC's) of all the detectors to signal the recording of event information. The computer reads out the ADC's and TDC's if an event has occurred.

Veto Scintillator Signals

The veto scintillator's PMT signals are delayed to allow for the trigger logic delays. The signals are then fed into multi-hit ADC's and TDC's. The computer reads out the ADC's and TDC's.

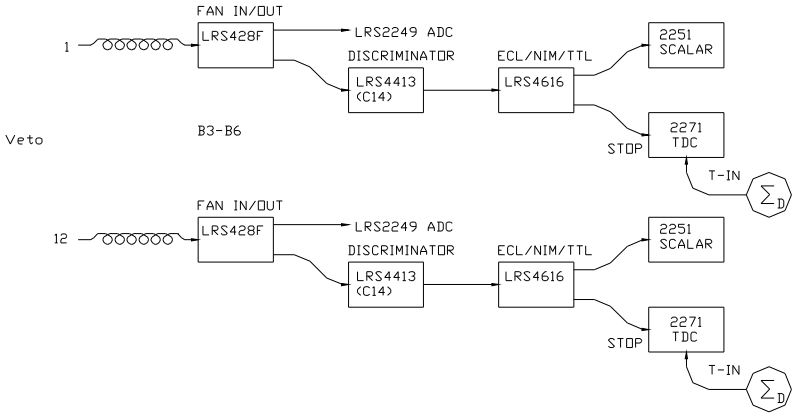

Figure 4.2 Veto scintillator ADC and TDC logic.

Wire Chamber Signals

Events in the wire chamber generate signals that are discriminated on the amplifier cards attached to the chamber. A threshold voltage is applied to all the cards and the output is an ECL logic pulse whose width corresponds to time over threshold. Each amplifier card is attached to 16 wires. The ECL pulses are then fed into Lecroy 4448 coincidence registers that record a logic 1 if a wire fired. The 4448 only records information that is coincident with the gate input of the module. The gate is generated by the trigger logic. The computer reads out the data stored in the 4448 registers for each event and stores the data for later processing.

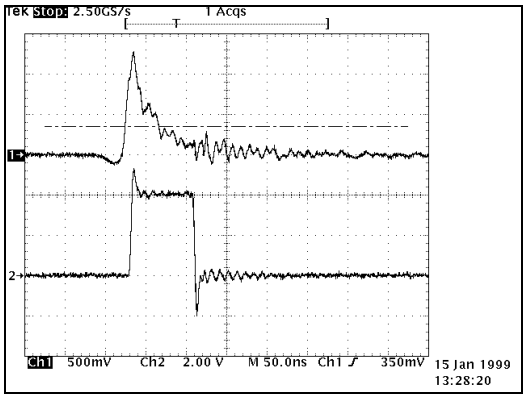

Figure 4.3: Typical input pulse using an 55Fe source and the corresponding ECL pulse output. The ECL pulse width corresponds to time over threshold of the input signal. Note that the input pulse is inverted in this figure. These pulses were taken directly from the amplifier card attached to the chamber with the detector in the lab at UGA.

Bench Testing

The completed chamber was bench tested in the lab using resistor cards to combine the signals from 16 wires. The current pulse is measured as the voltage across a ten meg-ohm resistor. Pulses were observed using a digital oscilloscope. A typical example of the pulses observed is shown in Figure 4.4.

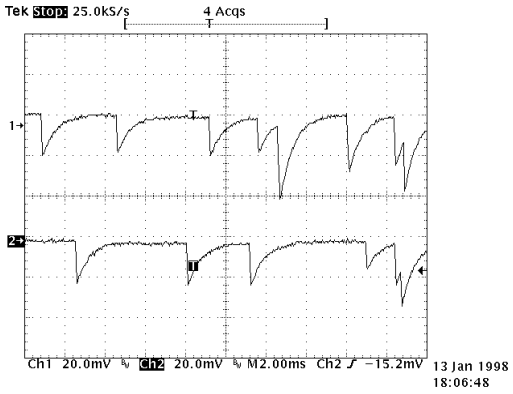

Figure 4.4 Typical voltage pulses for 16 wires terminated into a 1MΩ resistor. These pulses were the result of an 55Fe source. The upper signal is from the wire plane closest to the radioactive source and the lower signal from the other plane. Note that these signals are not correlated since the photons which result in a signal in one plane are destroyed and cannot generate a signal in the other. The last two pulses must be charged particles from cosmic rays since they are correlated in both time and amplitude.

The multiplication factor can also be determined experimentally by integrating the total charge in a typical output current pulse or by integrating the corresponding voltage pulse measured across a resistor.

(4.1) $$\zeta = \int_0^{3\tau} v(t)dt$$

Figure 5.2 shows an average voltage pulse along with its numerical integral obtained using a Tektronix digital oscilloscope. The measurement was made using an 55Fe source was used and the wires were terminated into a 1MΩ resistor.

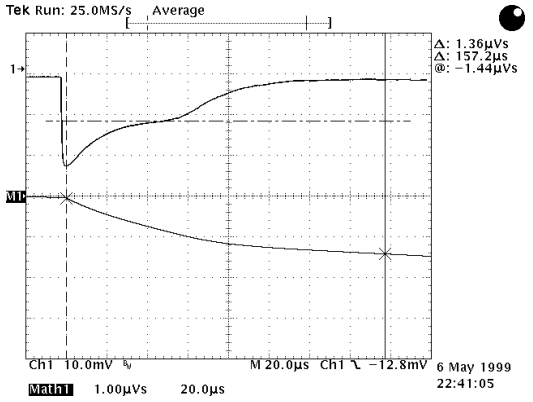

Figure 4.5 Typical pulse with the numerical integration on oscilloscope. Chamber voltage of 2900V with 80/20 Argon/CO2. Termination is 1 meg-ohm.

The relationship between the integrated pulse and the multiplication factor is where ζ is the integral of the voltage, R is the resistance, n_e is the number of electron-ion pairs and e_c is

(4.2) $$M = \frac{\zeta}{e_c n_e R}$$

the electron charge. 5.89 KeV photons from the 55Fe source produce on average $n_e = 227$ electrons yielding a multiplication factor of 4×10^4.

This same experimental technique can be used with a 90Sr source by integrating the average pulses from the β's radiation and dividing by the total number of electron-ion pairs formed along the track.

CHAPTER 5

Event Analysis

Overview

If the calorimeter detected an event then time and amplitude data was recorded for all the detectors using the analog to digital converters (ADC's) and the time to digital converters (TDC's). This data must be processed to extract useful information. The analog signals have pedestals that must be removed and gain must be matched for each photomultiplier tube. The pedestal is a fixed voltage output from the PMT that is a positive offset from the signal of interest. The signal is transmitted over long cables to the ADC's. There is a decrease in the amplitude of the signal due to the impedance of the cable. The pedestal is found in the data file to be the lowest recorded value from the ADC's for all the PMT's. It provides us with a measure of the loss in the cables and the connectors and ensures that we are measuring the entire analog signal. The gain of each PMT can then be determined by examining the energy distribution from each. The energy distribution should be the same and the gain is adjusted to ensure that this is the case.

Further processing of the TDC information is necessary to correlate events in all the detectors.

Finally using the known position of the detectors the path of a particle through the entire system can be determined.

Ultimately the path of the particle and the energy deposited is correlated with events in the hadron and electron spectrometers to calculate the kinematics of the reaction.

Lead Glass Gain Matching

The individual ADC readings must be adjusted to remove pedestals and to match the gain of the ADC's. The result is referred to as the gain-matched ADC values. Below is a superposition of histograms of ADC values before and after gain matching.

The pedestals and gain factors for the calorimeter blocks were determined from the recorded data and used to gain-match the data. The histograms shown in Figure 6.1 overlay the events from all 25 lead glass blocks. Ideally the hit count distribution would be the same for all the blocks. As can be seen some blocks were more efficient than others during the experiment.

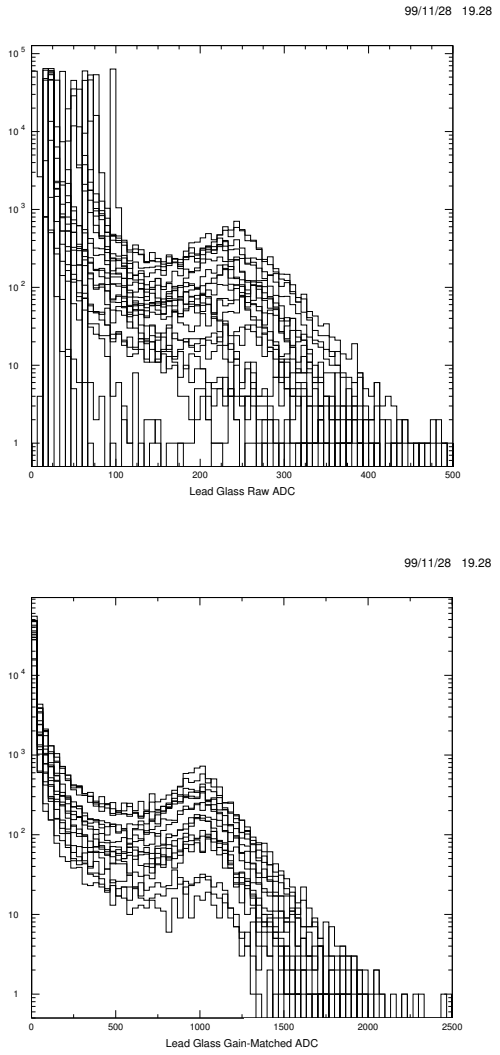

Figure 5.1 ADC spectrum before (above) and after (below) gain matching.

Table 5.1 lists the pedestals and gain factors for each of the glass blocks. The gain-matched ADC values directly correspond to the energy deposited in each glass block. Note that the PMT of block 16 was not functioning properly during the experiment.

Table 5.1 Pedestals and gain factors for the lead glass blocks.

Block #	Pedestal	Factor
1	96	5.584
2	37	4.684
3	75	4.630
4	66	5.249
5	68	5.5
6	74	5.583
7	50	4.885
8	47	5.585
9	23	5.184
10	24	5.132
11	62	4.973
12	32	5.587
13	52	5.237
14	54	5.349
15	18	5.044
16	24	5.2
17	20	5.867
18	25	6.081
19	19	5.982
20	21	4.955
21	17	5.2
22	21	5.830
23	23	4.550
24	2	5.2
25	16	4.826

Veto Scintillator Gain Matching

The ADC values must be gain matched as was done for the calorimeter ADC's. The TDC's are operated in common stop mode with each hit in a scintillator generating a stop signal. The hits in the veto that are completely uncorrelated to hits in the calorimeter result in a flat TDC time spectrum.

99/11/12 17.47

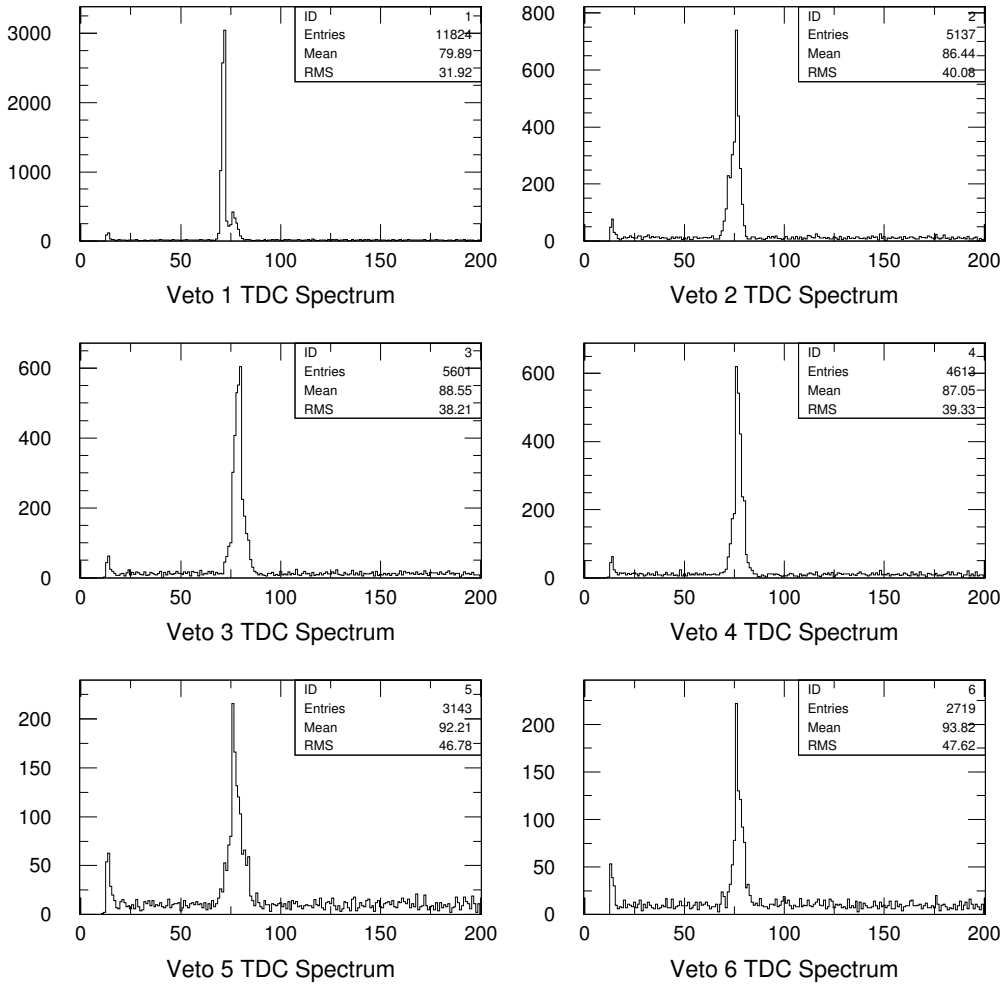

Figure 5.2 Veto scintillator TDC spectrum. The time between the peak on the far left and the main peak in the center is the signal propagation delay time. The hits along the baseline are random hits are therefore not correlated in time. The main peak exists because these hits occurred when a hit was detected coincidently in the calorimeter.

Hits that are the result of a particle passing through the veto and then entering the calorimeter are correlated in time. These hits show up in the distribution as a peak that occurs at a fixed time after the trigger signal that started the TDC.

This time delay corresponds to signal propagation delays in the circuitry. The recording of TDC values for each hit is necessary for reconstructing events in the detectors during off-line analysis.

Wire chamber analysis

Hits from the wire chamber were delayed approximately 150ns and recorded during a 300ns time window after the calorimeter detects an event. By delaying the signals from the wire chamber the logic circuitry can detect an event in the calorimeter and initiate the recording of hits in the wire chamber. A sample of the wire chamber hits is shown in figure 5.3.

Wires 48 and 51 were discovered to have fired during every event as can be seen in the figure above. Two different amplifier cards read out these two wires so the problem must be with the wires themselves. These must have been “hot wires” that have some problem that was causing a continuous signal.

Feedback in the amplifier cards themselves can be seen in figure 5.3 and appear as large group of wires firing. This feedback is the result of the high switching speed of the ECL signals generating noise that was picked up by the wires or the test input of the amplifier card. This feedback was observed in the lab to occur when the threshold voltage is low or due to cable routing/shielding problems.

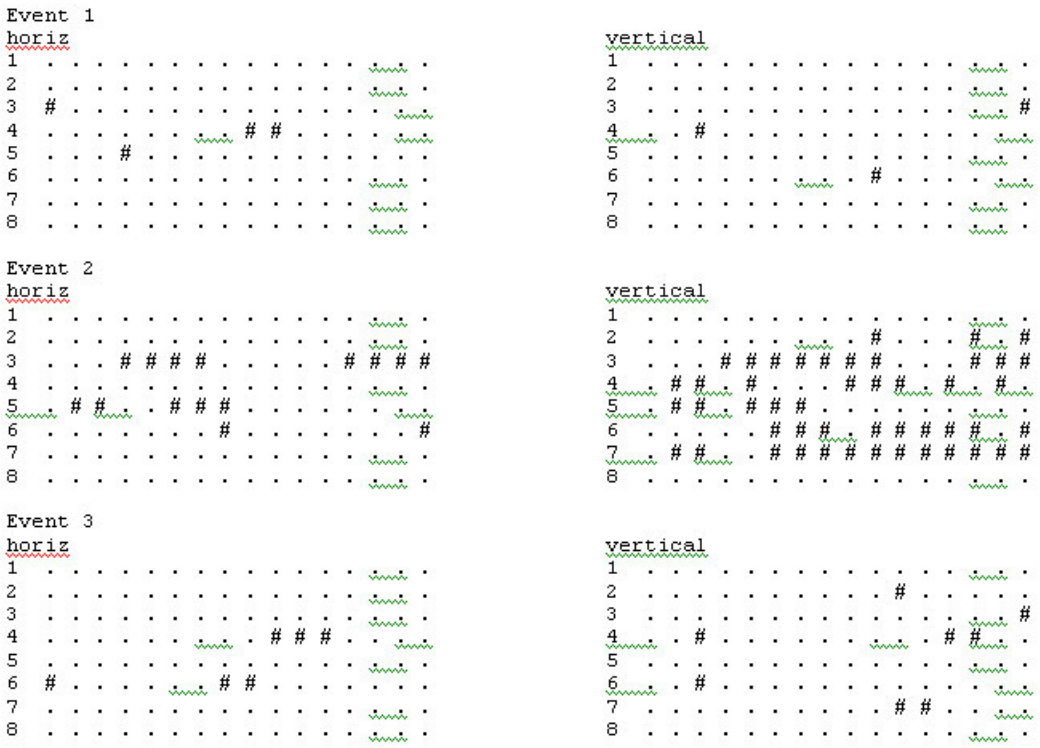

Figure 5.3 Sample of wire chamber hits for three events. Wire numbers 48 and 51 located on rows 3 and 4 of the vertical plane are always firing. The large number of hits for the second event hints that amplifier card feedback may be occurring.

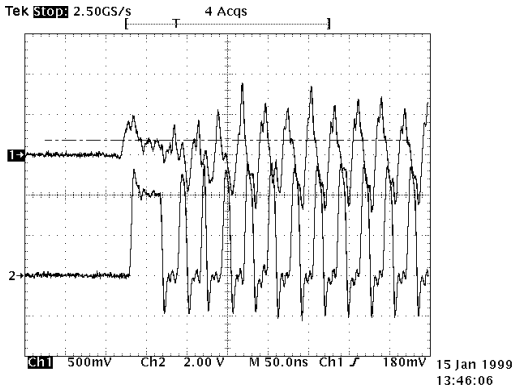

Figure 5.4 Onset of feedback. The upper signal is before the pre-amp section on the amplifier card. The lower signal is the ECL output signal.

It was discovered that grounding the test input of the amplifier card could prevent this feedback. The test input had to be grounded by soldering a very short wire between the test input and the nearest ground on the amplifier card itself. It was decided to verify that this problem occurs in the actual experiment before actually modifying all the cards.

CHAPTER 6

Event Discrimination

Detector Event Discrimination

To determine the performance of the wire chamber it is necessary to analyze the hits in each of the individual detectors in the photon arm. Requirements are placed in the software that impose conditions for valid hits corresponding to events in the calorimeter.

Calorimeter Events

Particles and photons arriving in the calorimeter produce electromagnetic showers, the photons from which were detected by phototubes attached to an array of 25 lead glass blocks. The phototubes in turn are connected to ADC's that record a value that is proportional to the fraction of energy deposited in each block by the shower.

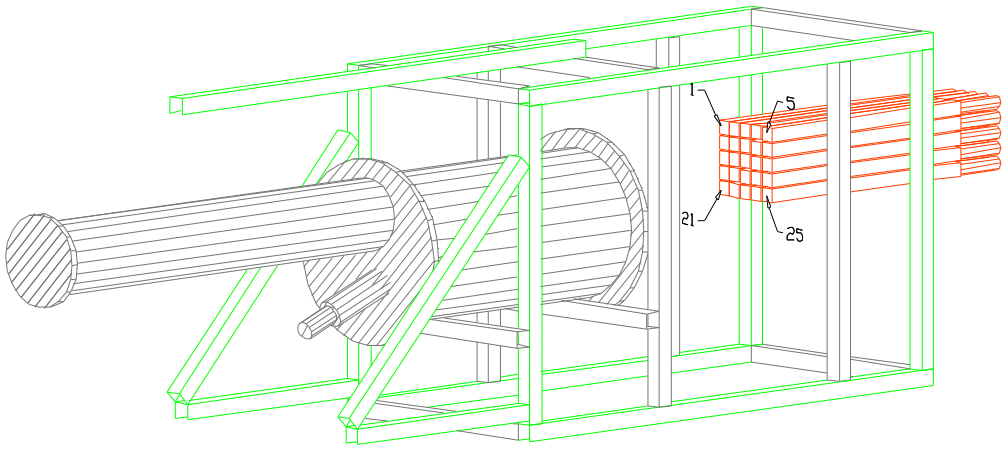

Figure 6.1 Calorimeter lead glass block numbering scheme.

The lateral extent of the electromagnetic shower is frequently represented as the sum of two gaussians and is approximately symmetric about the particle's original trajectory [10 p.137]. Therefore, the particle must have entered the calorimeter somewhere on the block in which the greatest amount of energy was deposited. This central block and its eight nearest neighbors are used to more precisely locate the event position. The hit position can be calculated using the energy weighted position of the nine blocks where x_i and y_i are the coordinates of the center of each

$$x = \frac{\sum_{i=1}^{9} x_i \ln(E_i)}{\sum_{i=1}^{9} \ln(E_i)} \qquad y = \frac{\sum_{i=1}^{9} y_i \ln(E_i)}{\sum_{i=1}^{9} \ln(E_i)} \tag{6.1}$$

block and E_i is the corresponding energy deposited in the ith block.

The second hit is determined to be the block that recorded the greatest amount of energy outside of the nine-block cluster associated with the first hit. Its eight nearest neighbors can be used to calculate the precise location of the second hit. The third hit is found in the same way by examining the blocks that were not used in the calculation of the first or second hits. Using this approach there can only be nine possible simultaneous hits taken into account for the 25 block array.

As can be seen in Figure 6.6 less than 3 percent of the photon arm events recorded two or more hits in the calorimeter. Therefore only the first and highest energy hit was used in the data analysis.

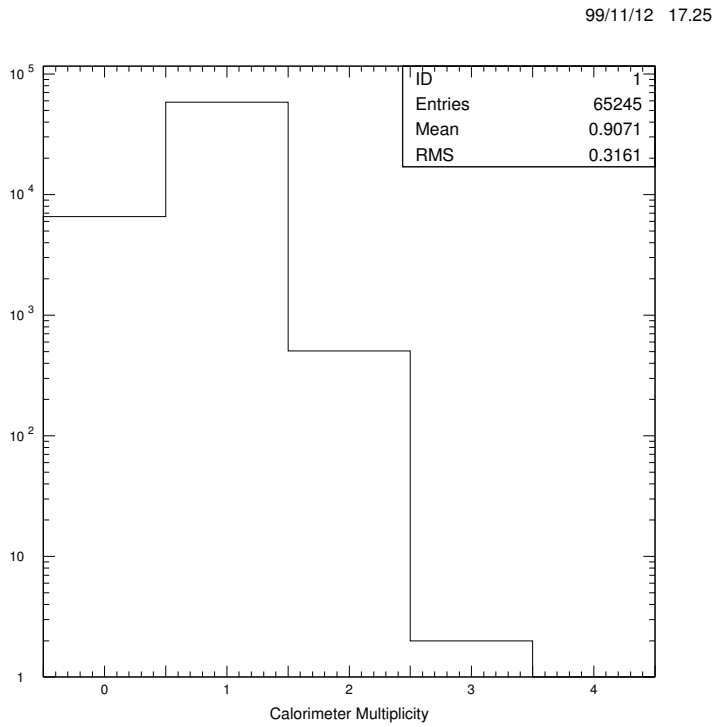

Figure 6.2 Calorimeter multiplicity.

An event was recorded when the energy deposited in the calorimeter exceeded a preset threshold value. Events consisted of the recording of all available hit information from all the detectors for later offline analysis.

Veto Scintillator Array Hits

TDC and ADC information is recorded for each hit of each element of the veto array. Multi-hit TDC's were used therefore multiple hits in a single veto scintillator were recorded. Valid hits in the veto are determined to be the timing of the hits that fall into a specific time window determined using the TDC.

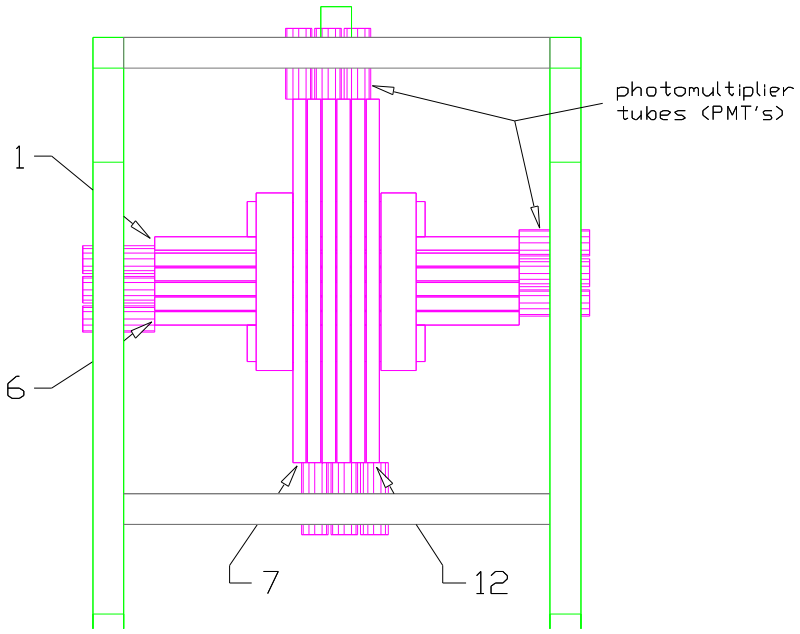

Figure 6.3 Veto scintillator numbering scheme as viewed from target.

The segmentation of the veto scintillators allow recording of separate x and y coordinates. This means that for two hits in the vertical and two hits in the horizontal that there are four possibilities for the coordinates of the two real particle tracks through the detector. If there are even more hits, then the problem becomes even more complex. To simplify matters, only events that recorded a single vertical and a single horizontal hit are used in the analysis.

The position of the hit is taken to be the center of each individual scintillator element.

Wire Chamber Events

LeCroy 4448 coincidence registers record hits in the wire chamber provided the hit occurred within an approximate 300ns gate after the hardware trigger. The software receives the information as a series of 16-bit values

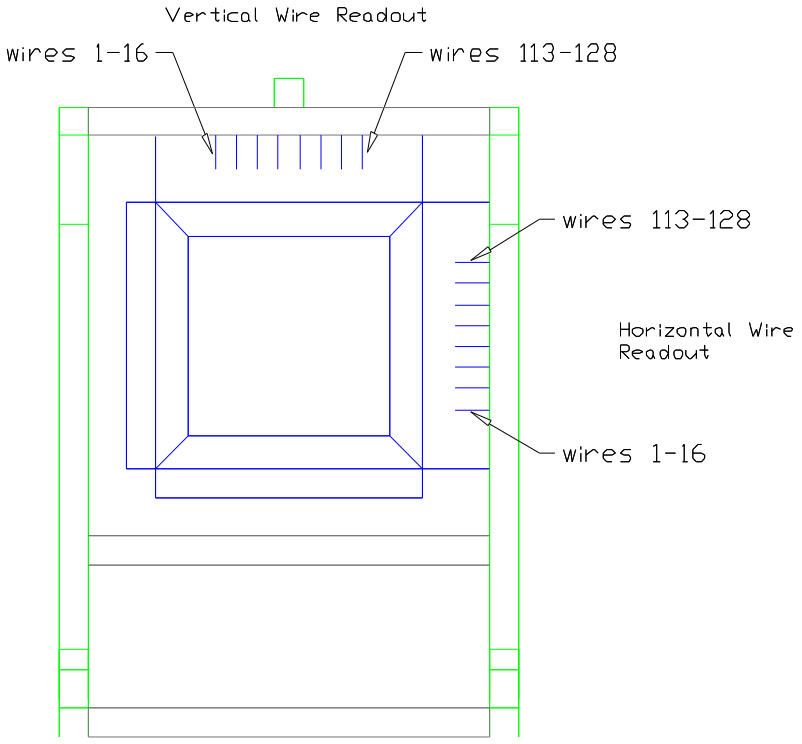

Figure 6.4 Wire chamber numbering scheme as viewed from target.

corresponding to groups of 16 wires. A hit in the wire chamber on a particular wire sets the bit corresponding to that wire.

The wire chamber analysis part of the program fills two 32-element arrays, one for the horizontal wires and the other array for the vertical wires, with the wire

numbers of the wires that fired. All information for a particular event is ignored if there was more than 32 hits in the wire chamber. The 300ns gate resulted in high

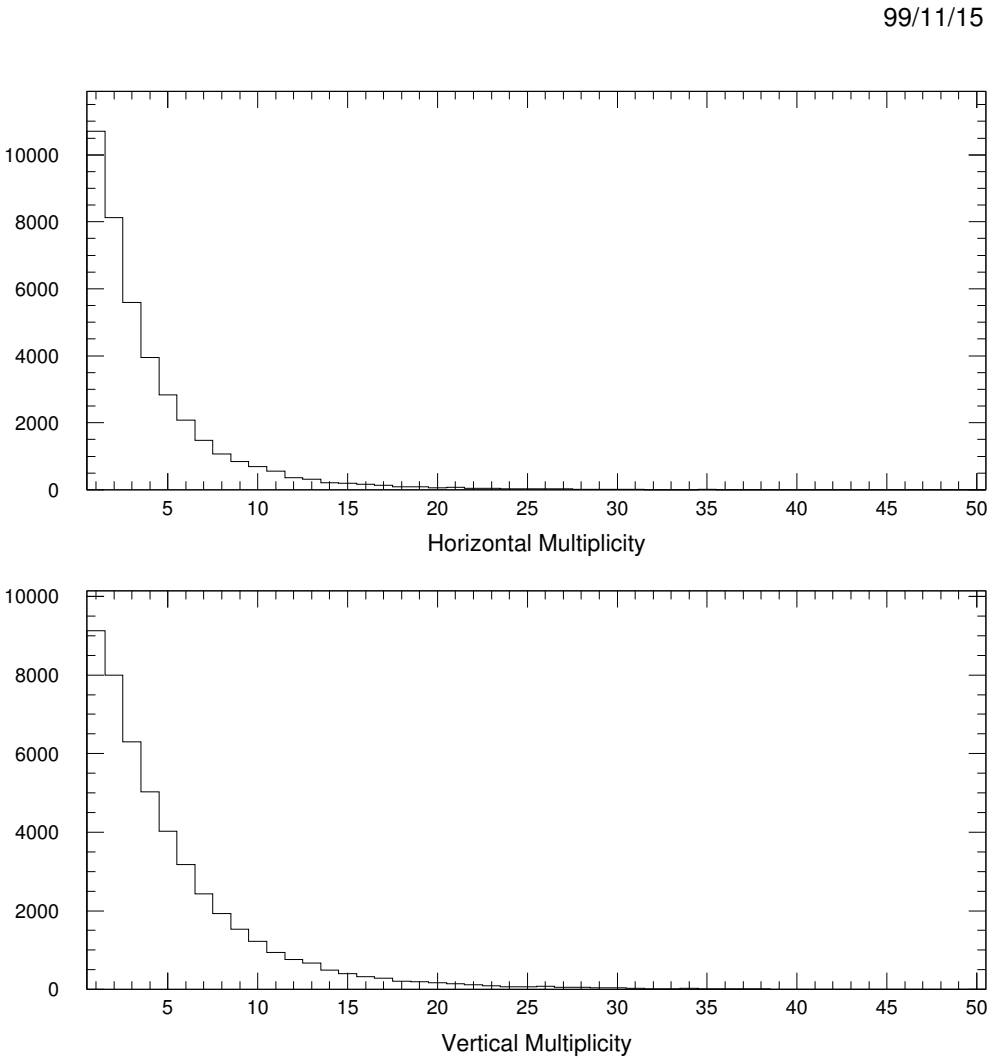

Figure 6.5 Wire chamber multiplicity

multiplicity for hits in the wire chamber. As can be seen in Figure the wire chamber multiplicity for the majority of events was ten or less.

There were two ‘hot’ wires that recorded hits for every event in the calorimeter. These two wires contribute to the inefficiency of the chamber since any particle that passes through the location of these two wires cannot be detected. Events that recorded very high multiplicity were examined and found to be most likely the result of oscillations due to feedback in the amplifier cards. These oscillations usually affect all the wires in a single plane masking any hits that may have occurred. As a result, all information for a particular event is ignored if there were more than 32 hits in the wire chamber.

Detector Position Calibration

Since the entire third arm is mounted on wheels and is rolled into place by pushing the assembly across floor then accurate pointing cannot be assumed. Also the relative positions of the individual detectors within the setup cannot be relied upon to be accurate. Therefore it is necessary to determine the relative position of the individual detectors.

The central axis of the photon arm is defined as the ray extending from the target to the center of the wire chamber. Positive values of x are in the direction of decreasing theta and positive values of y are in the direction of the floor. The actual position of the events in each detector were calculated using the relative offset of each axis of that detector and the spacing between each of the individual elements of each detector.

The position of each hit in the calorimeter is projected into the wire chamber and the miss distance is calculated for each axis to the nearest hit in the corresponding plane of the wire chamber. By plotting a histogram of the miss distance then the relative offset of the calorimeter is found to be the mean value of the miss distance. The offset was adjusted in the reconstruct.ini file until the mean was as close to zero as possible for the central block, No. 13. The spacing between the blocks was adjusted until the mean value of the miss distance in all the remaining blocks is zero.

The same process was applied to the veto scintillators.

Charged Particle Discrimination

Particle tracks through the detectors were reconstructed back to the target. A coincidence between a hit in the veto and a hit in the calorimeter is determined by projecting the hit in the calorimeter along the track back to the veto using similar triangles.

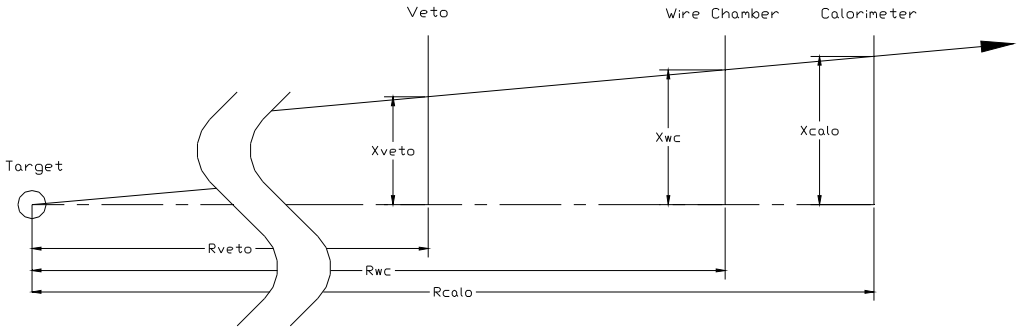

Figure 6.6 Projection of hits from calorimeter along particle track to veto.

Calculation of the projected hit in the veto is found using similar triangles.

$$x_{track} = x_{calo}\frac{d_{veto}}{d_{calo}} \qquad y_{track} = y_{calo}\frac{d_{veto}}{d_{calo}} \tag{6.2}$$

If the track through the veto meets the following conditions:

$$\left|x_{veto} - x_{track}\right| < \tfrac{1}{2} s_{x\,veto} \tag{6.3}$$

and

$$\left|y_{veto} - y_{track}\right| < \tfrac{1}{2} s_{y\,veto} \tag{6.4}$$

where s is the spacing between the veto elements then it is most likely that the event detected in the calorimeter was a charged particle. The electromagnetic shower resulting from a scattered electron in the calorimeter and the electromagnetic shower from a photon at GeV energies are indistinguishable. This is the reason for the need for veto detectors to reject the electrons. But the electron event data provides a very useful calibration information for the calorimeter. Since the electron can be detected in both the wire chamber and the calorimeter and it is known that the electron originated at the target then the track of the electron is known to the precision of the distance between the wires (2mm). This information is used in turn to verify the energy weighting and calibrate the central position of the electromagnetic shower in the calorimeter ensuring accurate trajectory information for photons that are not detected by the veto detectors.

CHAPTER 7

Wire Chamber Performance

Efficiency Determination

The efficiency of the wire chamber in recording the passage of a charged particle is determined by

$$Efficiency = \frac{N_{veto-calo-wire}}{N_{veto-calo}} \times 100\% \tag{7.1}$$

where $N_{veto-calo}$ is the number of coincidences between the calorimeter and the veto and $N_{veto-calo-wire}$ is the number of coincidences between all three detectors. If there was a coincidence between the veto and the calorimeter then a test is made on the hits in the wire chamber to determine if the wire chamber also recorded a hit. The track location in the wire chamber is calculated using

$$x_{track} = x_{calo} \frac{d_{wire\_chamber}}{d_{calo}} \qquad y_{track} = y_{calo} \frac{d_{wire\_chamber}}{d_{calo}} \tag{7.2}$$

and the closest wire chamber hit must be within the limit

$$x_{wire\_chamber} - x_{track} < 2\sigma_{calo} \tag{7.3}$$

or for the horizontal wires

(7.4) $$y_{wire\_chamber} - y_{track} < 2\sigma_{calo}$$

to count as a coincidence. Each plane of the wire chamber is tested individually yielding efficiency data for each.

If a charge particle was detected then the coordinate of the projected hit in the wire chamber is recorded in a histogram of predicted hits. If the closest hit recorded in the wire chamber falls within the limits give by Equations

(7.3) $$x_{wire\_chamber} - x_{track} < 2\sigma_{calo}$$

and

(7.4) $$y_{wire\_chamber} - y_{track} < 2\sigma_{calo}$$

then the coordinate of the projected hit is recorded in a histogram of actual wire chamber hits. The predicted hits histogram is divided by the histogram of actual wire chamber hits resulting in a histogram of the efficiency of the wire chamber as a function of wire number.

CHAPTER 8

Conclusion

The wire chamber efficiency was found to be excellent for both planes. The trailing off of the efficiency of the y plane as a function of increasing wire number was the result of the veto scintillators extending beyond the active area of the wire chamber. This resulted in events being recorded that may have passed through the active region of the chamber or may have missed the active region but still passed through the scintillators and recorded an event in the calorimeter.

The results of the tests of this chamber in Hall A have proven that it can survive the high particle background and still record useful data for calibrating the position of hits in the calorimeter and rejecting charged particles.

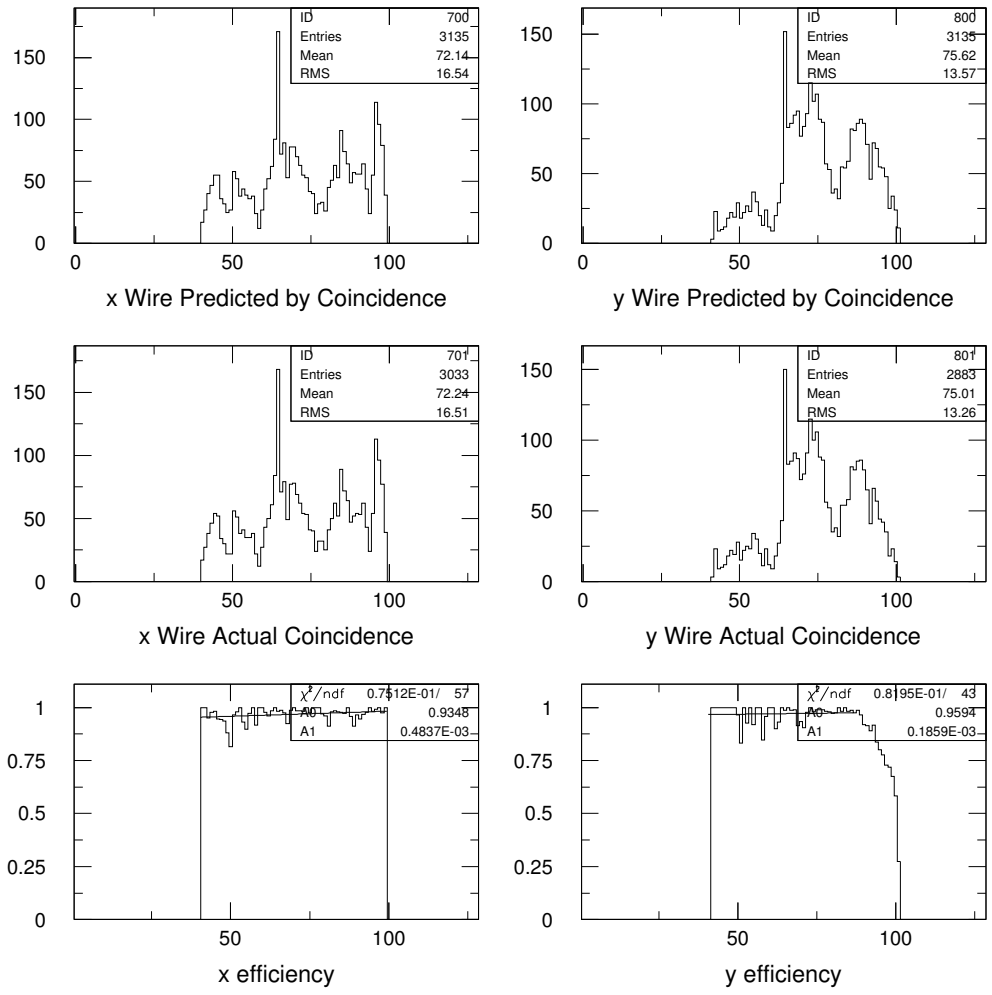

Figure 8.1 Wire chamber efficiency.

REFERENCES

[1] F.F. Rieke and W. Prepejchal, Phys. Rev. A6 (1972) 1507

[2] C.H. Yoder, F.H. Suydam and F.A. Snavely, Chemistry (Harcourt Brace Jovanovich, Atlanta, Ga. 1975)

[3] H. Fischle, J. Heintze and B. Schmidt, Experimental Determination of Ionization Cluster Size Distributions in Counting Gasses, Nuclear Instruments and Methods in Physics Research, A301 (1991) 202-214

[4] F. Sauli, Principles of Operation of Multiwire Proportional and Drift Chambers, Lectures at CERN (1977)

[5] J.C. Armitage, S.P. Beingessner, R.K. Carnegie, E.F. Ritchie and J. Waterhouse, A Study of the Effect of Methane and Carbon Dioxide Concentration on Gas Amplification in Argon Based Gas Mixtures, Nuclear Instruments and Methods in Physics Research, A271 (1988) 588-596

[6] W. Blum and L. Rolandi, particle detection with drift Chambers (Springer-Verlag, Berlin, Germany 1994) p. 131, pp 125-127

[7] Personal communication with Circuit Board Mfr in Atlanta and Kepco Circuit Systems

[8] H. Fenker, A Standard Beam PWC For Fermilab, TM-1179 2557.000 (1983)

[9] H. Tolsma, The Honeycomb Strip Chamber, Ph.D. Thesis, NIKEF 1996

[10] Review of Particle Physics, July 1999